Chemical Engineering Journal Advances 8 (2021) 100154

Contents lists available at ScienceDirect

Chemical Engineering Journal Advances

journal homepage: www.sciencedirect.com/journal/chemical-engineering-journal-advances

Modeling molecular structure and behavior of microbial extracellular polymeric substances through interacting-particle reaction dynamics

Run-Ze Xu [a], Jia-Shun Cao [a], Ganyu Feng [a], Jing-Yang Luo [a], Yang Wu [b], Bing-Jie Ni [c], Fang Fang [a,*]

[a] Key Laboratory of Integrated Regulation and Resource Development on Shallow Lakes, Ministry of Education, College of Environment, Hohai University, Nanjing 210098, China
[b] State Key Laboratory of Pollution Control and Resource Reuse, School of Environmental Science and Engineering, Tongji University, 1239 Siping Road, Shanghai 200092, China
[c] Centre for Technology in Water and Wastewater (CTWW), School of Civil and Environmental Engineering, University of Technology Sydney (UTS), Sydney, NSW 2007, Australia

ARTICLE INFO

Keywords:
extracellular polymeric substances
interacting-particle reaction dynamics
computational biology
extraction
microbial aggregates
averaged concentration representation method

ABSTRACT

Extracellular polymeric substances (EPS) are essential for bacteria to interact with external environments and play a key role in the formation of microbial aggregates. Unveiling the black box of EPS has become an urgent topic in the field of microbiology, medical science and environmental science. Here, we develop an explicit approach to describe the molecular structure and behaviors of EPS using interacting-particle reaction dynamics (iPRD). Three representative states of EPS (*i.e.*, normal EPS layer, metal bridging EPS layer and extracted EPS layer) are qualitatively simulated at molecular scale and validated with previous research results on EPS. Furthermore, an averaged concentration representation method is proposed to quantitatively model the EPS-oriented bioprocesses. Through this method, the contents of protein and polysaccharide in EPS extracted by cation exchange resin are accurately predicted by our model (R^2>0.982). This work gives new insights into EPS at the molecular scale and opens up new avenues for further exploring and modeling complex molecular structure and behaviors of EPS.

1. Introduction

Extracellular polymeric substances (EPS), which are heterogeneous viscous matrix originated from bacteria, mainly consist of polysaccharides, proteins, humic substances, extracellular DNA (eDNA), and inorganic substances [1, 2]. In the past decades, EPS have drawn much attention due to their significant functions in the formation of microbial aggregates [3, 4]. On one hand, EPS crucially affect the formation of microbial biofilms due to the sticky substances in EPS [4, 5]. EPS also affect the transformation of substrates via the various functional groups in EPS [6]. Inhibiting the production of EPS has been recognized as a promising method to prevent and eliminate microbial biofilm in many industrial and biomedical applications [4, 5]. On the other hand, the performance of membrane technology in wastewater treatment processes is significantly influenced by membrane fouling caused by the accumulation of EPS on membrane [7-9]. Nonetheless, EPS still suffer from an identity crisis due to the lack of comprehensive methods for recovery and characterization of EPS [1]. As a result, the existing mathematical models for EPS normally treat EPS as a whole and depend on concentration-based modeling approaches such as the Monod equation and stoichiometric matrix [10-12]. For instance, Ni et al. (2009) [11] considered EPS as a particulate component (X_{EPS}) in their mechanistic model for microbial products of activated sludge. Peng et al. (2019) [13] also simplified EPS as the X_{EPS} and simulated the variation of X_{EPS} in anammox biofilm. These models cannot simulate the spatial structure of EPS and help us further investigate the molecular scale features related to EPS. However, these features are closely associated with the functions and molecular behaviors of EPS, which need to be considered in explicit molecular models to further explore the secrets of EPS. Although many functions and structural features of EPS have been deduced based on previous researches [14], the explicit model for simulating the molecular structure and behaviors of EPS is still missing.

Interacting-particle reaction dynamics (iPRD) have been developed to simulate the reaction kinetics in crowded environments of biological cells [15, 16]. Molecular dynamics simulations are embedded in the

* Corresponding author.
E-mail address: ffang65@hhu.edu.cn (F. Fang).

https://doi.org/10.1016/j.ceja.2021.100154
Received 21 May 2021; Received in revised form 8 July 2021; Accepted 9 July 2021
Available online 11 July 2021

Abbreviation list

MV	Membrane vesicles
DS	Dissolved substrate
UPN	Unlinked protein
UPS	Unlinked polysaccharide
MC	Metal cation
iCER	Ions released from cation exchange resin
LB	Lipid bilayer
MVFS	Membrane vesicles formation site
CPPN	Channel protein for protein
CPPS	Channel protein for polysaccharide
MPN	Membrane protein
MPS	Membrane polysaccharide
LPN	Linked protein
LPS	Linked polysaccharide
EBPS	Enzyme-binding polysaccharide
E	Enzyme
MBMPN	Metal-binding MPN
MBMPS	Metal-binding MPS
MBLPN	Metal-binding LPN
MBLPS	Metal-binding LPS

iPRD model to simulate complex interactions among particles [17, 18]. In such simulations, for example, realistic kinetics of biomembranes [15], protein binding patterns [19], and kinetics of bimolecular reactions [20], these particles can represent atoms, higher-order molecules, and even large polymers. The bimolecular reaction simulated by the iPRD model is a two-step process, in which two active particles converge in the diffusion process and subsequently react with a user-defined probability [16]. The iPRD model allows topology simulation and general interaction potentials on the reactive particles, such as steric repulsion and electrostatic forces [17], which govern the interactions among polymers in EPS [1]. For instance, the proteins and humic substances with chelating groups in EPS were found to effectively bind heavy metals through electrostatic forces [7]. The carboxyl group, hydroxyl group, and RC-O-CR in glucoside of EPS were also found to hinder the transfer of plasmid-borne antibiotic resistance genes through electrostatically binding [21]. The motion of particles and microscopic reactions between them in three-dimensional space can be explicitly simulated by the iPRD model [17]. Therefore, the iPRD model may be a useful tool to simulate both the formation and behaviors of polymers in EPS layers.

In this study, we propose an explicit molecular modeling to simulate the molecular structure and behaviors of EPS based on the iPRD model [17]. The microscopic information of EPS layers for establishment of the iPRD model was introduced firstly. Then, the detailed structure of the particle-based computational model for EPS layers was explained. With the help of the iPRD model, the three different equilibrium states of EPS layers were simulated. We also demonstrate the feasibility of using the iPRD model to quantitatively simulate important bioprocesses occurred in the EPS layers. An averaged concentration representation method is developed to simulate the content of EPS polymers extracted by cation exchange resin (CER). This work presents potential applications in understanding and quantitatively modeling complex molecular behaviors of EPS at the molecular scale.

2. Materials and methods

2.1. Particle-based computational model

In the particle-based computational model for EPS layers, all polymers or metal cations are modeled as spherical particles. The particle dynamics are simulated by the overdamped Langevin dynamics with isotropic diffusion. A particle *i* defined in this system moves according to the stochastic differential equation:

$$\frac{dx_i(t)}{dt} = -\frac{D_i(T)}{k_B T}\mathbf{f}_i(t) + \sqrt{2D_i(T)}\xi_i(t) \tag{1}$$

where $x_i(t) \in \mathbb{R}^3$ is the particle position at time t, $D_i(T)$ is a specific diffusion coefficient for each particle type, k_B is the Boltzmann constant (1.380649×10^{-23}J/K), T is the system temperature (K), $\mathbf{f}_i(t)$ is the deterministic force and $\xi_i(t)$ is the stochastic velocity.

A harmonic repulsion potential is used to describe the interaction between two hydrophobic-dominant particles. It makes two particles repulse each other once they enter a certain radius. The potential term is given by

$$V(x_1, x_2) = \begin{cases} \frac{1}{2}k(\|x_1 - x_2\|_2 - r)^2, & if \quad \|x_1 - x_2\|_2 < r, \\ 0, & otherwise, \end{cases} \tag{2}$$

where r is the distance (nm) at which particles begin to interact with respect to this potential.

A screened electrostatic potential is used to model the interaction between two charged particles. It represents electrostatic interaction (both repulsive or attractive), which is screened with a certain screening depth. The potential term is given by

$$V(\|x_1 - x_2\|_2) = V(r) = \begin{cases} \frac{C}{r}e^{-kr} + D\left(\frac{\sigma}{r}\right)^n, & if \ r \le r_c, \\ 0, & otherwise, \end{cases} \tag{3}$$

where $C \in \mathbb{R}$ is the electrostatic repulsion strength (kJ*nm/mol), $k \in \mathbb{R}$ is the inverse screening depth (1/nm), $D \in \mathbb{R}$ is the repulsion strength (kJ/mol), $\sigma \in \mathbb{R}$ is the core repulsion radius or zero-interaction radius (nm), $n \in \mathbb{N}$ is the core repulsion exponent, and $r_c \in \mathbb{R}$ is the cutoff radius (nm).

In this study, the units of length, time and energy were defined as nanometer, second and kilojoule per mol, respectively. The simulation temperature was set according to the simulation target. The polymers within EPS layers share a complex liquid environment, and few pieces of research focused on the diffusion constants of different polymers in the EPS matrix. Therefore, the default diffusion constants of linked substances were accepted, which varied with the simulation temperature (Eq. (1)). In order to simulate the structure of the microbial cell membrane, the diffusion constants of membrane compositions (i.e. LB, MVFS, CPPN and CPPS) were set as 0. Compared with low diffusion constant of topology species, the free particles have much higher diffusion constant. The low diffusion constant presented the fixation and aggregation of EPS on microbial cell membranes, whereas the higher diffusion constant showed the rapid movement of free particles in a well-mixed liquid environment. In the ReaDDy 2 model, the reaction rates (λ) have units of inverse time (1/s) and can be understood as the probability per unit time of the reaction occurring [17]. When two particles are closer than a reaction radius, the reaction between them will happen with probability:

$$p = 1 - e^{-\lambda\tau} \tag{4}$$

where τ is the integration step. The practical reaction rates were defined based on the comparison between simulation results and experimental results.

2.2. Averaged concentration representation method

In the iPRD model, the concentrations of proteins, polysaccharides, and dissolved substrates were calculated based on their density (ρ) and varying total volume (Table S1). The mean density of proteins was 1.37 g/cm^3 while the mean density of polysaccharides was set as 1.60 g/cm^3,

which is the density of alginic acid (Aladdin, A110570, CAS: 9005-32-7). The acetate was chosen as a representative dissolved substrate, which has a density of 1.05 g/cm^3 (Aladdin, A298827, CAS: 64-19-7). The simulation box with the size of x × y × z = 50nm × 10nm × 100nm had a volume of 5.0 × 10^{-20} L. The size of simulation box defined in this study depended on the thickness of the capsular EPS layer between the cell membrane of *Defluviicoccus* sp. [22] (Fig. S1). To fully illustrate the interactions between EPS and other extracellular substances, the size of simulation box in z-direction was extended to 100 nm. The concentrations of simulated particles in EPS layers were calculated as follows:

$$C_i(t) = \frac{\rho_i n_i(t) V_i}{V_S} \quad (5)$$

where $C_i(t)$ is the concentration of particle type i at time t, ρ_i is the density of particle type i, $n_i(t)$ is the numbers of particle type i at time t, V_i is the volume of single particle type i, and V_S is the total volume of the simulation box (5.0 × 10^{-20} L). A heterotrophic microbial cell with a radius of 250 nm was chosen as the model bacteria, which was wrapped by the EPS layer and interacted with external environments. The microbial cell has a volume of 6.5 × 10^{-17} L, and the sphere with a radius of 350 nm has a volume of 1.8 × 10^{-16} L. Therefore, the volume of total simulation boxes reached 1.15 × 10^{-16} L, and the total numbers of simulation boxes on one cell reached 2300. As a result, all experimental results need to be averaged before comparing them with the simulation results of the iPRD model.

2.3. Data source of EPS extraction experiment

The detailed description of EPS extraction experiments can be found in Frølund et al. (1996) [23]. Briefly, raw activated sludge was collected from aerated tanks in the advanced treatment plant (Aalborg East), and the supernatant of activated sludge was removed to thicken sludge with total solids of 8-11 g/L. The thickened sludge was centrifuged to remove any EPS from bulk water, and subsequently, the sludge pellets were resuspended in a buffer consisting of 2 mM Na_3PO_4, 4 mM NaH_2PO_4, 9 mM NaCl and 1 mM KCl at pH 7. In the extraction process, 300 mL sludge was transferred to an extraction beaker with baffles and a specific amount of CER (85g/g VS, DOWEX 20-50 mesh in the sodium form) was added. The stirring intensity was set as 900 rpm, and different extraction times (0.5-17 h) were chosen. The extracted EPS were harvested by centrifugation to remove CER and remaining floc components.

2.4. Software

The particle-based reaction-diffusion simulator (ReaDDy 2) is mainly implemented in C++ while the detailed models were encoded in the python user interface such as Jupyter notebook. The python interface can help users compose the simulation system, define particles, potentials and reactions, as well as run, store and analyze simulations [17]. The step by step tutorials of the ReaDDy 2 can be found online (https://readdy.github.io/). The software package Visual Molecular Dynamics (VMD) is used for visualizing the simulation results and recording the number and coordinates of particles [24]. The color and texture of each particle type in the snapshots of VMD were user-defined. A more detailed description of the ReaDDy 2 model can be found in the *Supporting Information*.

3. Results and discussion

3.1. Microscopic information of EPS layers

In the past few decades, researchers have utilized different *in situ* microscopic technologies, such as Scanning Electron Microscope (SEM) [22, 25], Transmission electron microscopy (TEM) [22, 25], Atomic Force Microscope (AFM) [26], and Confocal Laser Scanning Microscope (CLSM) [9, 26], to capture the microscopic structure of EPS adsorbed on microbial cells. These valuable pictures supply useful information about EPS layers including the thickness of the EPS layer, the spatial structure of EPS subcomponents, and specific functions of each kind of subcomponent. These previous studies on EPS provide a strong foundation for us to build a reasonable iPRD model for EPS layers.

As shown in Fig. S1, the thickness of the capsular EPS layer between the cell membrane of *Defluviicoccus* sp. and the liquid environment reached 20-40 nm [22]. In order to model complex properties and behaviors of EPS, the thickness of 40 nm was accepted as a normal thickness of simulated EPS layers. The proteins, polysaccharides and extracellular DNA (eDNA) are the most common subcomponents of EPS identified by CLSM [9, 26, 27]. In the EPS layers, the key proteins normally contain two types, namely, amyloid proteins [28] and extracellular enzymes [29]. The chemical structure of amyloid proteins is folded as β-sheets and stacked vertically to the fibril axis [28]. The amyloid proteins secreted by *Escherichia coli* are 4-12 nm wide and 0.1-10 μm long [30]. Therefore, the radius of structure proteins defined in the iPRD model was set as 4 nm. The extracellular enzymes have the ability to hydrolyze external macromolecules, and are adsorbed on the polysaccharide skeleton in EPS [31]. Membrane vesicles (MV) are actively produced by bacteria to deliver the extracellular enzymes [31, 32]. In the iPRD model of EPS, the extracellular enzymes were encapsulated in the MV. When the MV encountered the polysaccharide skeleton in the EPS layers, the enzymes were released from MV and bound with the polysaccharide skeleton. Therefore, the radius of MV and extracellular enzymes were defined as 5 nm and 4 nm, respectively.

The polysaccharide skeleton of EPS consists of many types of polysaccharides, such as alginate, cellulose, xanthan, and chitin [33, 34]. These polysaccharides have both negative charge and hydrophobic properties, which support the connection between polysaccharide and other substances, for example, proteins or metal cations [35]. The hydrolysis of polysaccharides in EPS by amylase greatly hindered bacterial aggregation and reduced the stability of anammox granule [36], indicating that the polysaccharide skeleton of EPS has significant structural functions. Abu-Lail and Camesano (2003) [37] reviewed the size of different polysaccharides detected by AFM, and alginate, as the most common polysaccharide in EPS, is 1.41-4.65 nm wide (single strands). Thus, the radius of structural polysaccharide was set as 1.5 nm in this study.

The eDNA in EPS present significant functions in the formation of microbial biofilms, such as binding with proteins, delivering information between cells, and maintaining biofilm structure [26, 27, 31]. The polymethylmethacrylate coated with DNase I enzyme strongly reduced the adhesion of *Staphylococcus aureus* (95%) and *Pseudomonas aeruginosa* (99%), indicating the key role of eDNA in biofilm formation [5]. However, in the present iPRD model, the informative function of eDNA cannot be modeled, and the communication between two microbial cells is beyond our model scope. Meanwhile, the structural functions of eDNA in EPS are very similar to those of proteins and polysaccharides [38]. The simulation of proteins and polysaccharides can reasonably show the structural functions and behaviors of EPS. Therefore, eDNA was not modeled in this study. In addition, humic substances are normally identified from microbial EPS and originate from the lysis of microbial cells [39]. The humic substances are refractory to biodegradation and possess the function of electron transport [40]. In this study, the microbial lysis was not simulated, and consequently, the humic substances were not included in our model at present. The summaries of the iPRD model parameters for constituting EPS are summarized in Table 1.

3.2. A particle-based computational model for EPS layers

In the previous section, the model settings of subcomponents in EPS and corresponding reasons were discussed. Here, the detailed information about the iPRD model of EPS established by the particle-based reaction-diffusion simulator (ReaDDy 2) was demonstrated [17]. In

Table 1
Key configuration of the iPRD model for simulating different states of EPS layers.

Simulation target	Temperature	Timestep	Numbers of timesteps	Numbers of particles[a]	Numbers of reactions[b]
Normal EPS layer	293 K	0.001 s	120000	Particle species: 1, 2, 3, 4. Topology species: 7, 8, 9, 10, 11, 12, 13, 14, 15, 16.	Particle reactions: 1, 2, 3, 4, 5. Topology reactions: 14, 15, 16, 17, 18, 19, 20, 21, 22, 23.
Metal bridging EPS layer	293 K	0.001 s	120000	Particle species: 1, 2, 3, 4, 5. Topology species: 7, 8, 9, 10, 11, 12, 13, 14, 15, 16, 17, 18, 19, 20.	Particle reactions: 6, 7, 8, 9.
Extracted EPS layer	293 K	0.001 s	120000	Particle species: 1, 2, 3, 4, 5, 6. Topology species: 7, 8, 9, 10, 11, 12, 13, 14, 15, 16, 17, 18, 19, 20.	Particle reactions: 10, 11, 12, 13.
EPS extraction process	277 K	0.01 s	720000	Particle species: 6. Topology species: 13, 14, 19, 20.	Particle reactions: 12, 13.

[a] The detailed description of particle types can be found in Table S2 and S3.
[b] The detailed description of reaction types can be found in Table S4 and S5.

previous studies, the pictures from SEM and TEM show that EPS wrap microbial cells like a capsule [22]. Except for water molecules and hydrophilic polymers, the different subcomponents of EPS are stacked and linked to each other through electrostatic or hydrophobic interaction [2]. To understand the connection patterns and microbial behaviors of EPS layers, a cross-section with size of x × y × z = 50nm × 10nm × 100nm was simulated in the iPRD model (Fig. 1a). The boundaries of the simulation box can be either non-periodic or fully periodic. The polymer that existed in one cross-section of the EPS layer may connect with other polymers in neighboring cross-sections (Fig. 1b). In this case, the simulated cross-section of the EPS layer is periodic in ***x*** and ***y*** directions but not in ***z*** direction.

The topology species and topology types, which were used to build complex multi-particle structures, can be defined in the iPRD model [17]. Therefore, the particles in simulated EPS layers were divided into free particles (Table S2) and topology species (Table S3). The free particles moved "freely" in EPS layers and liquid environments. The membrane vesicles (MV), dissolved substrate (DS), unlinked protein (UPN), unlinked polysaccharide (UPS), and metal cation (MC) were set as free particles. Due to the lack of hydrodynamic simulation in the ReaDDy 2, the hydrodynamic conditions of free particles (*i.e.* mixing by stirring or aeration) were simulated by adjusting diffusion coefficient (*D*). A high diffusion coefficient endows free particles high magnitude of random displacement in the governing dynamics, which simulates a well-mixed hydrodynamic condition.

The topology species were divided into four topology types according to their identities. The *Membrane* type described the compositions of the microbial cell membrane (Fig. 2a), initial linked proteins and polysaccharides (Fig. 2b, c), which included lipid bilayer (LB), membrane vesicles formation site (MVFS), channel protein for protein (CPPN), channel protein for polysaccharide (CPPS), membrane protein (MPN) and membrane polysaccharide (MPS). These compositions of microbial membrane are assembled through the harmonic potential to restrict the movement of the membrane components. When DS encounters MVFS, CPPN or CPPS within a certain radius, the DS will be converted to MV, UPN or UPS, respectively (Fig. 2d). These processes simulated the absorption of nutrients and the release of specific substances by microbial cells. The *Structure* type contained linked protein (LPN) and linked polysaccharide (LPS), which constituted the main structure of the EPS layer (Fig. 2e). The *Enzyme* type presented the connection between enzyme and polysaccharide skeleton. When MV encounters LPS, enzyme (E) will be released from MV, and LPS will be converted into enzyme-binding polysaccharide (EBPS) (Fig. 2f). The final topology type was named *Bridge*, which described the electrostatic interaction between metal cations (MC) and negatively charged polymers. When MC collides negatively charged polymers (*i.e.,* MPN, MPS, LPN and LPS), the MC and these polymers will merge into metal-binding polymers: metal-binding MPN (MBMPN), metal-binding MPS (MBMPS), metal-binding LPN (MBLPN) and metal-binding LPS (MBLPS) (Fig. 2g).

The reaction processes occurring and the symbols for particles in the simulated EPS layers are summarized in Fig. 2. Particle reactions included secretion and hydrolysis processes, whereas the topology spatial reactions contained hydrophobic connection, enzyme binding, metal bridge, and CER extraction processes. The reaction radius was defined according to the radius of two reactants and the potential between them (Table S4 and S5).

CER has been widely used to extract EPS by exchanging metal cations bound with EPS [23, 41]. The CER normally has a radius of 0.5-1.0 mm, which is too large to be simulated by the iPRD model. Therefore, the addition of CER was simplified as ion released from CER (iCER), which had a radius of 0.1 nm and had the function of exchanging MC in metal-binding polymers (Fig. 2h).

For free particles, many types of pair potentials, such as harmonic repulsion, weak interaction piecewise harmonic, Lennard-Jones potential, and screened electrostatics, can be modeled in the iPRD model [17]. In this study, the potential of particles without charge was set as

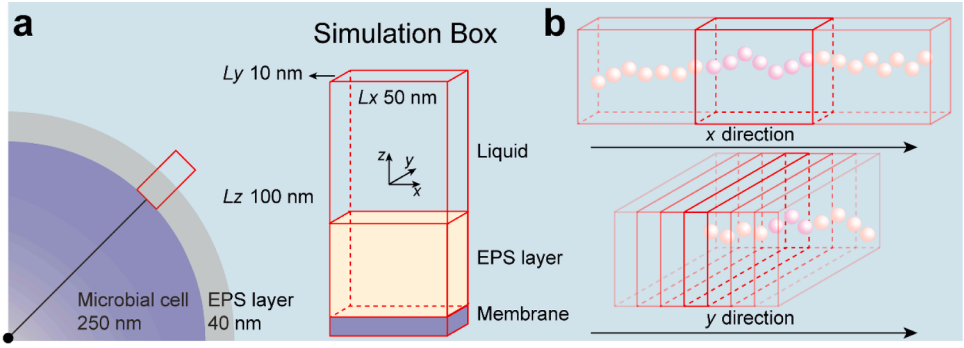

Fig. 1. The illustration of simulation box for the EPS layer. a The simulated microbial cell had a radius of 250 nm and was wrapped by the EPS layer with a mean thickness of 40 nm. The simulation box with size of x × y × z = 50nm × 10nm × 100nm was randomly placed on the surface of the microbial cell. Due to the small length in both ***x*** and ***y*** directions, the bottom of the simulation box was assumed to be a flat surface rather than a curved surface. **b** The EPS layer was composed of numerous continuous simulation boxes in both ***x*** and ***y*** directions. The polymers (spheres) in the target simulation box may (1) connect with polymers in neighboring simulation boxes, (2) come from neighboring simulation boxes, (3) leave the target simulation box. In order to simulate these phenomena, the simulation box was periodic in ***x*** and ***y*** directions but not in ***z*** direction.

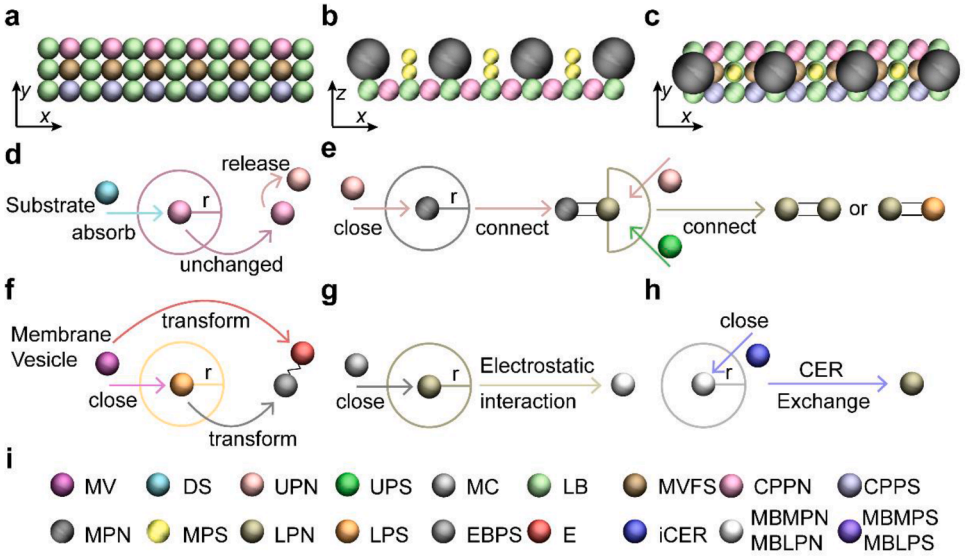

Fig. 2. Initial membrane structure, particle reactions, and topology spatial reactions embedded in the iPRD model. a The top view of the membrane structure taken from the iPRD model. Three types of special membrane sites were defined in a topology type and assumed to absorb substrates and release specific substances. **b-c** The front and top view of proteins and polysaccharides initially bound to the membrane, which provide initial adsorption sites for other polymers. **d-h** The particle reactions and topology spatial reactions defined in the iPRD model. **d** The DS close to the CPPN was absorbed and the UPN was released by the microbial cell. The DS close to the MVFS and CPPS had similar reactions. **e** The UPN close to the MPN was transformed to the LPN and was connected with the MPN. The UPN and the UPS close to the LPN were transformed into LPN and LPS, respectively. Then, they were connected with each other. **f** The MV close to the LPS was transformed to E and the LPS was transformed to EBPS. The EBPS was recognized as the binding skeleton for enzymes. **g** The MC close to the LPN was combined with the LPN through electrostatic interaction and transformed the LPN to the MBLPN. The MPN, MPS and LPS also had a similar reaction with the MC. **h** The iCER close to the MBLPN exchanged the MC in the MBLPN and transformed the MBLPN to the LPN. The MBMPN, MBMPS and MBLPS also had a similar reaction with the iCER. **i** The symbols for particles simulated in the iPRD model. The unified radius was used to present these symbols in this figure while the actual radius was applied in the model snapshots. The signs and corresponding definitions of components were summarized in the abbreviation list.

harmonic repulsion, which hindered the overlap of particles. Meanwhile, the particles with charge interacted with each other through screened electrostatics. The characteristics of harmonic potential (Table S6) and screened electrostatics (Table S7) were determined based on the radius of two particles and previous researches for these potentials [42]. The bonds among topologies species are defined on pairs of particles, angles on triples, and dihedrals on quadruples. In this study, harmonic bonds between two topology species were defined according to the topology types and species (Table S8). When the topology types and species are changed through topology spatial reactions, the characteristics of harmonic bonds will be changed accordingly.

3.3. *Qualitative simulation of equilibrium states of EPS layers*

Based on the iPRD model, three different equilibrium states of EPS layers were simulated (Fig. 3): (a) Normal EPS layer: the EPS layers with a thickness close to 40 nm contained structural proteins, polysaccharides, and active enzymes. (b) Metal bridging EPS layer: the structural proteins and polysaccharides in EPS layers were bridged by metal cations. (c) Extracted EPS layer: the metal cations in EPS layers were exchanged by CER, and partial structural proteins and polysaccharides were extracted from the EPS layers by stirring.

The initial membrane structure with MPN and MPS constituted the base of the EPS layer, and the centers of the membrane formed the horizontal plane with a height of 0 nm (Fig. 3a). As shown in Fig. 3a, the simulated EPS layer had a vertical structure with a maximum thickness of 38.2 nm. The LPN and LPS stacked on the microbial membrane and were linked with the MPN and MPS. The hydrophobic and electrostatic interactions governed the interactions among them [36], and consequently, a relatively large distance (> 2 nm) between two particles was observed [42].

Note that the maximum thickness of the normal EPS layer originated from the extracellular enzymes (E: red particle). The simulated enzymes had a function of hydrolyzing the macromolecules and represented the active ingredients in EPS. In order to hydrolyze the external macromolecules and avoid self-degradation of extracellular enzymes, the main part of extracellular enzymes normally located at the outer layer of EPS [43]. The extracellular polysaccharides such as alginate [31] and sialic acids [44] in EPS provide the binding sites for extracellular enzymes and have the ability to protect EPS polymers and microbial cells from attack by proteases or glycosidases [44]. In our model, the E particles were tightly bound with the EBPS (grey particle) and were located in the outer layer of EPS, which were consistent with the previous experimental results and theoretical analysis [31, 44, 45].

The metal bridging EPS layer was modeled based on the simulation results of the normal EPS layer. The addition of MC and the development of metal bridging reactions started the transition from negatively charged polymers to metal-bound polymers (white and purple particles in Fig. 3b). In contrast to the sparse distribution of polymers in Fig. 3a, the distribution of polymers bound with MC was more crowded due to the metal bridging (Fig. 3b), which greatly shorten the distance between two particles from >2 nm to ~1 nm. As a result, the simulated maximum thickness of the metal bridging EPS layer reduced from 38.2 nm to 36.3 nm.

After the extraction of EPS by CER and continuous stirring, the polymers in EPS were isolated from the membrane structure (Fig. 3c). The addition of CER can exchange the MC bound with the negatively charged polymers and reduce the effects of metal bridging [23]. Then, the simulated stirring process separated polymers in EPS from the membrane structure by endowing the disconnected LPN (brown particles) and LPS (orange particles) high diffusion constants. The extracted EPS also exhibited the aggregation property, which was agreed with high molecular weights (kDa) of extracted EPS in the previous researches [46, 47].

To clearly present the effects of metal bridging and CER extraction, the locations (z coordinate of particle center) of main subcomponents in three simulated EPS layers were illustrated in Fig. 3d-f. The maximum height of LPN in Fig. 3a reached 25.3 nm while the maximum height of MBLPN in Fig. 3b was reduced to 21.1 nm due to the metal bridging (Fig. 3d). Similarly, the MBLPS became more crowded than the LPS (Fig. 3e). The locations of extracellular enzymes were also closer to the microbial membrane after the addition of MC (Fig. 3f). The z coordinates of the extracted EPS layer were much higher than that of the two former simulated EPS layers, indicating that the EPS were well-extracted by the

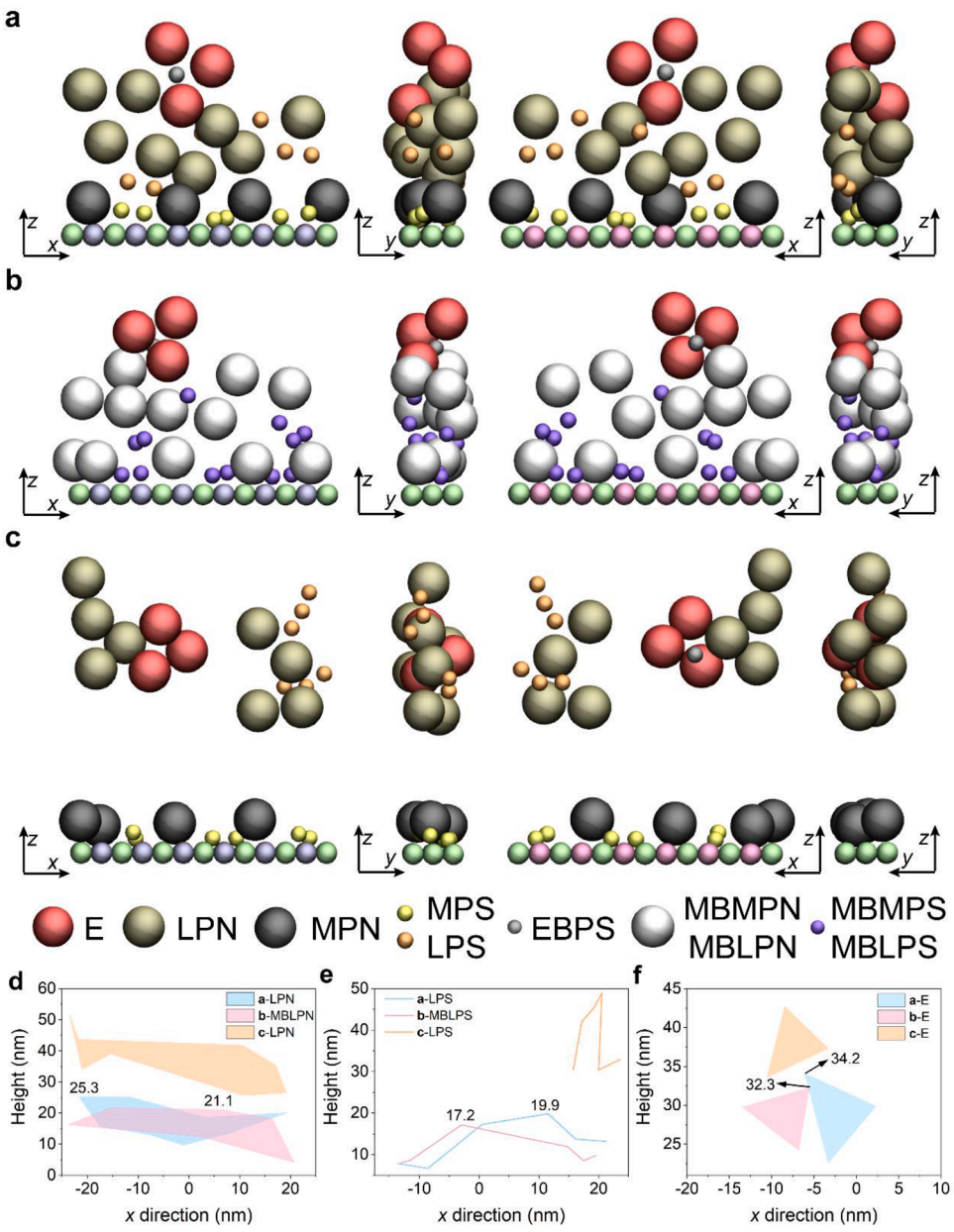

Fig. 3. Snapshots of three different equilibrium states of EPS layers taken from the iPRD simulations. a Snapshots of normal EPS layer in four directions. The hydrophobic interactions and electrostatic repulsion governed the interactions among the simulated particles. The distance between the two particles was normally larger than 2 nm. **b** Snapshots of metal bridging EPS layer in four directions. The combination between the MC and the negative charged polymer caused the metal bridging, which shortened the mean distance between two particles from 2 nm to 1 nm. **c** Snapshots of extracted EPS layer in four directions. The MCs bound with the negative charged polymers were exchanged by the ions released from the cation exchange resin (CER). The dosage of CER and continuous stirring (high diffusion constants for EPS polymers) separated the EPS from the microbial membrane. **d** The varying locations of simulated structural proteins in three different equilibrium states of EPS layers. The height of 0 nm was set as the center of membrane particles. **e** The varying locations of simulated structural polysaccharides in three different equilibrium states of EPS layers. **f** The varying locations of simulated enzymes in three different equilibrium states of EPS layers. The signs and corresponding definitions of components were summarized in the abbreviation list.

CER and stirring method.

3.4. Quantitative simulation of dynamic states of EPS layers

Extracting EPS from microbial cells is essential for us to characterize, quantify, and even recover EPS [1]. Unfortunately, an optimal and unified extraction method for EPS is still missing at present. In the past decades, researchers have explored different EPS extraction methods including chemical, physical and mixed methods. The mathematical analysis and optimization of EPS extraction methods normally depended on the simple kinetic analysis or response surface methodology [48]. The iPRD model for predicting the yield of EPS during the EPS extraction process is yet to be established. Among all extraction methods for EPS, extracting EPS by CER is one of the most common extraction methods used in recent studies [6, 32, 49, 50], and its EPS yield is usually compared with other extraction methods [8, 51]. The CER can extract EPS through the ions exchange process and this process has been qualitatively simulated in the previous section. Therefore, in this section, we purpose to establish an iPRD model for quantitatively predicting the yield of EPS in the CER extraction process, which involves delicate molecular behaviors of EPS.

Based on the averaged concentration representation method, the varying concentrations of EPS during the CER extraction process were predicted by the iPRD model. The yield of EPS via CER extraction was affected by the dosage of CER, the stirring intensity and the extraction time [23]. The sodium ions are released from the sodium-form CER via ion exchange channels, and subsequently exchange the calcium or manganese ions within EPS polymers (Fig. 4a). The distribution of EPS polymers will become sparser due to the lack of metal bridging (Fig. 3a, c). A relatively high stirring intensity can accelerate the mixing of mixed liquid and the separation of sparse EPS polymers. In the iPRD model, the dosage of CER (g/g volatile solid (VS)) was controlled by the addition of iCER and the stirring intensity was controlled by the adjustment of diffusion constants. The total cell numbers of activated sludge in this EPS extraction experiment were 5×10^{11}cells/gVS [23]. Therefore, the unit of concentration can be approximatively transformed from mg/g VS to mg/cell. Then, the varying concentrations of subcomponents in the single simulation box can be calculated according to the total numbers

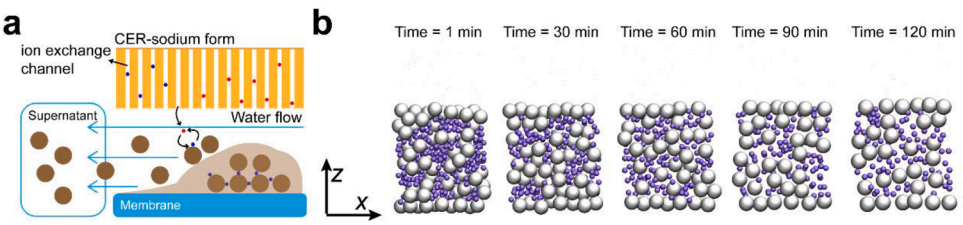

Fig. 4. The theoretical and simulated EPS CER-extraction process. a The theoretical EPS CER-extraction process. The sodium form CER release sodium ions through ion exchange channels to exchange metal ions bound with EPS polymers. Then, the EPS polymers with negative charged become looser, and are separated from the membrane due to the water flow with high disturbance intensity. **b** The snapshots of simulated EPS CER-extraction process from 1 to 120 min. The numbers of the MBLPN (white particles) and the MBLPS (violet particles) decreased over time due to the extraction by the iCER (red particles, small particles with radius of 0.1 nm).

of simulation boxes on each model cell.

We assumed that the original EPS polymers were bound with metal cations (*i.e.* MBMPN and MBMPS), which widely existed in external liquids, such as trace element nutrient solutions and wastewater. The snapshots of the EPS extraction process from 1 min to 120 min are illustrated in Fig. 4b. During the EPS extraction process, the numbers of MBLPN and MBLPS polymers in the simulation box decreased because of the iCER exchange reaction. The red particles in the upper space of the simulation box represented iCER, which freely moved depending on the mixed conditions. The lower space of the simulation box was occupied by the crowded EPS polymers, which were confined in the space with *z* coordinate from -50 nm to 0 nm. The extracted EPS polymers disappeared due to their high diffusion constants, indicating that the extracted EPS polymers left the simulation box and stayed in the supernatant (Fig. 4b). The decreased numbers of EPS polymers were converted to the increased concentrations of extracted EPS. The averaged values of 8 times simulation were compared with the experimental results (Fig. 5). The simulated concentrations of both proteins and polysaccharides showed high consistency with the actual observations (R^2>0.982), which demonstrated the feasibility to simulate the EPS extraction process via the iPRD model. The mechanism of particle-based prediction was different from that of mechanistic models. The former depends on the characteristics of reactive particles, reaction rates, and diffusion constants, whereas the latter assumes that the reactants are totally mixed [10]. The probability-based models are more consistent with the actual situations of microbial environments [16], and the rapid development of computational power in the 21st century ensures its operability. Therefore, our simulated results demonstrated that the iPRD model has the potential to qualitatively and quantitatively simulate more complex molecular structures and behaviors of EPS.

3.5. *Practical implications and prospects*

The molecular structure of the EPS layers was successfully simulated by our model. The normal EPS layer simulated in this study presented the equilibrium state of EPS between the microbial membrane and external liquid environments (Fig. 3a). The model of normal EPS layer can be further improved to simulate different biochemical processes such as mass transfer in the EPS layer, hydrolysis and absorption of various macromolecules by EPS, and microbial response to external toxic chemicals. The simulation of metal bridging EPS layer represented a common phenomenon that metal bridging between metal ions and negatively charged polymers can enhance the aggregation of polymers (Fig. 3b) [2, 52]. In the iPRD model, the decrease of molecular distance can be simulated by the change of topology types and their band length (Table S3 and S5). With the help of topology functions, more complex

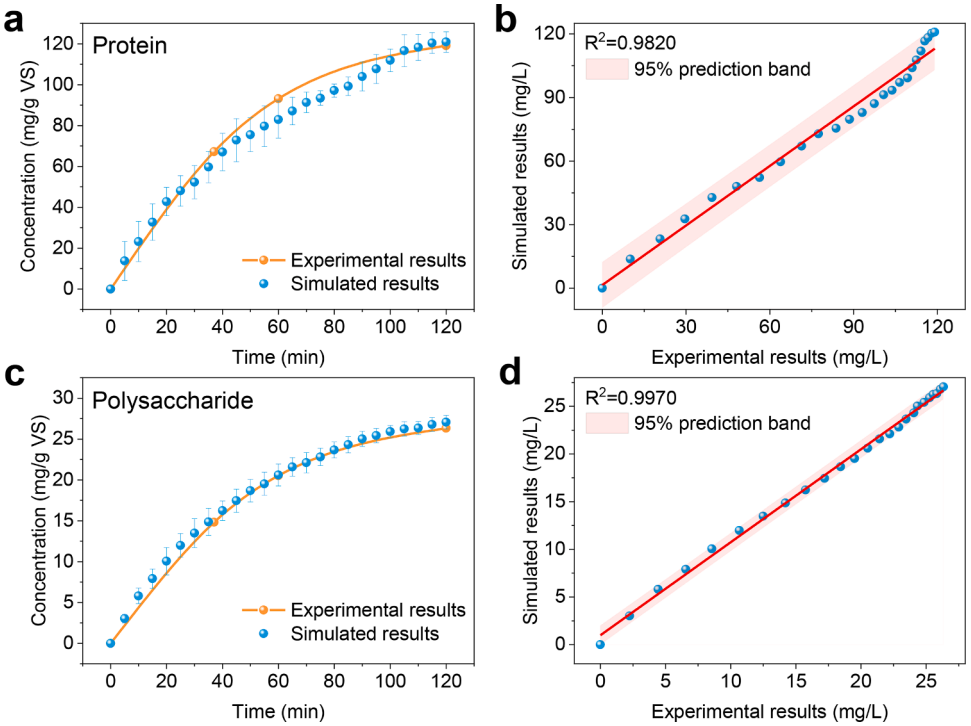

Fig. 5. Predicting the EPS yield of the CER-extraction process. a The comparison between simulated concentrations of extracted proteins and experimental results. **b** The linear fit between simulated results and experimental results of extracted proteins. **c** The comparison between simulated concentrations of extracted polysaccharides and experimental results. **d** The linear fit between simulated results and experimental results of extracted polysaccharides.

interactions within EPS layers such as binding heavy metals [53], transferring extracellular electrons [54] can be modeled. The qualitative simulation of EPS layers at equilibrium proved the capability of the iPRD model in exploring the spatial structure of EPS and potential interactions within EPS.

Besides that, our work also validated the feasibility of the iPRD model in quantitively simulating biochemical processes occurred in the EPS layers. For quantitative simulation, the metabolism of microbial communities and the external conditions need to be averaged to the single cell level. To save the calculation cost, the simulation space of single cell was further reduced to numerous simulation boxes with fixed volume (Fig. 1). The averaged concentration representation method (see detailed descriptions in Method) developed in this study endowed probability-based models the ability of numerical simulation, which is the specialty of mechanistic models [11, 12]. To achieve a more accurate simulation, we can divide the simulated polymers into smaller particles with aggregated interactions, whereas the calculation cost will greatly grow due to the increase in the number of particles.

Moreover, the flexibility of the iPRD model can help us establish more delicate and complex biophysical processes related to EPS [16, 17]. For example, the interactions between EPS and surface topography of antimicrobial materials can be modeled by simulating the special surface topography as functional particles. These interactions are essential to minimize microbial infections and biofilm formation on material surfaces, which is an important problem in many areas including in medicine and biomaterials engineering [55]. Furthermore, in environmental science and technology, EPS play a crucial role in many pollutant remediation processes, especially in biofilm and membrane bioreactor technology [7]. We can simulate different types of pollutants, such as heavy metals, microplastics, macromolecular chemicals, as particles with different properties. Then, the interactions between these particles and EPS can be quantitively predicted by the iPRD model. The iPRD models also have the potential to model some interesting intercellular communication and regulation processes, such as quorum sensing regulation [56], antibiotic resistance gene transfer [21], and extracellular electron transfer [54]. Of course, to simulate these complex biophysical processes, more experiments at single cell level are necessary [57]. More potential functions of the iPRD models can be explored by future experiments about the molecular insight of EPS [7].

In addition, there are some limitations existed in this model. Firstly, the hydrodynamic conditions were modeled based on the adjustment of diffusion constants rather than a specific hydrodynamic module, because the hydrodynamic interactions are not included in the ReaDDy 2 simulator at present [17]. Secondly, the model of the EPS extraction process ignored the disturbance from the lysis of microbial cells. Although the optimal extraction conditions for EPS need to ensure the integrity of all cells, almost all extraction experiments cannot meet this requirement [8, 50, 51, 58]. The lysis of microbial cells can be identified by the detection of extracellular DNA [50], the measurement of G6DPH activity in EPS extracts [51], or fluorescence staining by the BacLight cell viability kit [51]. The third limitation is that the current model only considered the interface between the microbial membrane and liquid environments. The biophysical processes occurred in the interface between the microbial membrane and material surface, or the interface between two microbial cells are possible to be simulated by the iPRD model in our future research.

4. Conclusions

In this study, an explicit approach based on interacting-particle reaction dynamics (iPRD) was developed to characterize molecular structure and behaviors of microbial EPS. This approach simulated the extracellular components of EPS as different particles and defined the interactions between them. With the help of the iPRD model, we were successful in qualitatively modeling three equilibrium states of EPS, and quantitatively modeling the EPS extraction process via CER. The process of model establishment was demonstrated in detail, which could help researchers further utilize this model to study their own topics on EPS. Therefore, our work has promising applicability for illustrating EPS at the molecular scale and opening up new avenues for exploring and modeling complex molecular structures and behaviors of EPS.

Declaration of Competing Interest

The authors declare that they have no known competing financial interests or personal relationships that could have appeared to influence the work reported in this paper.

Acknowledgements

We thank the National Natural Science Foundation of China (51878244, 51878243), the Fundamental Research Funds for the Central Universities (B200202101), and the Priority Academic Program Development of Jiangsu Higher Education Institutions (PAPD), China for supporting this work.

Supplementary materials

Supplementary material associated with this article can be found, in the online version, at doi:10.1016/j.ceja.2021.100154.

References

[1] T. Seviour, N. Derlon, M.S. Dueholm, H.C. Flemming, E. Girbal-Neuhauser, H. Horn, S. Kjelleberg, M.C.M. van Loosdrecht, T. Lotti, M.F. Malpei, R. Nerenberg, T.R. Neu, E. Paul, H. Yu, Y. Lin, Extracellular polymeric substances of biofilms: suffering from an identity crisis, Water Res. 151 (2018) 1–7.
[2] Y. Tian, L. Zheng, D.-Z. Sun, Functions and behaviors of activated sludge extracellular polymeric substances (EPS): a promising environmental interest, J. Environ. Sci. 18 (2006) 420–427.
[3] W. Wang, Y. Yan, Y. Zhao, Q. Shi, Y. Wang, Characterization of stratified EPS and their role in the initial adhesion of anammox consortia, Water Res. 169 (2020), 115223.
[4] L. Dieltjens, K. Appermans, M. Lissens, B. Lories, W. Kim, E.V. Van der Eycken, K. R. Foster, H.P. Steenackers, Inhibiting bacterial cooperation is an evolutionarily robust anti-biofilm strategy, Nat. Commun. 11 (2020) 11.
[5] J.J.T.M. Swartjes, T. Das, S. Sharifi, G. Subbiahdoss, P.K. Sharma, B.P. Krom, H. J. Busscher, H.C. van der Mei, A Functional DNase I Coating to Prevent Adhesion of Bacteria and the Formation of Biofilm, Adv. Funct. Mater. 23 (2013) 2843–2849.
[6] F. Fang, R.Z. Xu, S.N. Wang, L.L. Zhang, Y.Q. Huang, J.Y. Luo, Q. Feng, J.S. Cao, Characterization of interactions between a metabolic uncoupler O-chlorophenol and extracellular polymeric substances of activated sludge, Environ. Pollut. 247 (2019) 1020–1027.
[7] H.Q. Yu, Molecular insights into extracellular polymeric substances in activated sludge, Environ. Sci. Technol. 54 (2020) 7742–7750.
[8] Z. Liang, W. Li, S. Yang, P. Du, Extraction and structural characteristics of extracellular polymeric substances (EPS), pellets in autotrophic nitrifying biofilm and activated sludge, Chemosphere 81 (2010) 626–632.
[9] S.-Q. Ni, N. Sun, H. Yang, J. Zhang, H.H. Ngo, Distribution of extracellular polymeric substances in anammox granules and their important roles during anammox granulation, Biochem. Eng. J. 101 (2015) 126–133.
[10] C.S. Laspidou, B.E. Rittmann, A unified theory for extracellular polymeric substances, soluble microbial products, and active and inert biomass, Water Res 36 (2002) 2711–2720.
[11] B.J. Ni, F. Fang, B.E. Rittmann, H.Q. Yu, Modeling microbial products in activated sludge under feast-famine conditions, Environ. Sci. Technol. 43 (2009) 2489–2497.
[12] B.J. Ni, B.E. Rittmann, F. Fang, J. Xu, H.Q. Yu, Long-term formation of microbial products in a sequencing batch reactor, Water Res 44 (2010) 3787–3796.
[13] L. Peng, H.H. Ngo, S. Song, Y. Xu, W. Guo, Y. Liu, W. Wei, X. Chen, D. Wang, B. J. Ni, Heterotrophic denitrifiers growing on soluble microbial products contribute to nitrous oxide production in anammox biofilm: model evaluation, J. Environ. Manage. 242 (2019) 309–314.
[14] P. Zhang, B. Feng, Y.-P. Chen, Y.-Z. Dai, J.-S. Guo, In situ characterizations for EPS-involved microprocesses in biological wastewater treatment systems, Crit. Rev. Env. Sci. Tec. 49 (2019) 917–946.
[15] M. Sadeghi, F. Noé, Large-scale simulation of biomembranes incorporating realistic kinetics into coarse-grained models, Nat. Commun. 11 (2020) 2951.
[16] T.M. Earnest, J.A. Cole, Z. Luthey-Schulten, Simulating biological processes: stochastic physics from whole cells to colonies, Rep. Prog. Phys. 81 (2018), 052601.
[17] M. Hoffmann, C. Frohner, F. Noe, ReaDDy 2: Fast and flexible software framework for interacting-particle reaction dynamics, PLoS Comput. Biol. 15 (2019), e1006830.

[18] R.J. Najmanovich, J. Schöneberg, F. Noé, ReaDDy - a software for particle-based reaction-diffusion dynamics in crowded cellular environments, PLoS ONE 8 (2013).
[19] J. Schoneberg, M. Heck, K.P. Hofmann, F. Noe, Explicit spatiotemporal simulation of receptor-G protein coupling in rod cell disk membranes, Biophys. J. 107 (2014) 1042–1053.
[20] M. Dibak, C. Frohner, F. Noe, F. Hofling, Diffusion-influenced reaction rates in the presence of pair interactions, J. Chem. Phys. 151 (2019) 13.
[21] X. Hu, F. Kang, B. Yang, W. Zhang, C. Qin, Y. Gao, Extracellular polymeric substances acting as a permeable barrier hinder the lateral transfer of antibiotic resistance genes, Front. Microbiol. 10 (2019) 736.
[22] M. Pronk, T.R. Neu, M.C.M. van Loosdrecht, Y.M. Lin, The acid soluble extracellular polymeric substance of aerobic granular sludge dominated by Defluviicoccus sp, Water Res 122 (2017) 148–158.
[23] B. Frølund, R. Palmgren, K. Keiding, P.H. Nielsen, Extraction of extracellular polymers from activated sludge using a cation exchange resin, Water Res 30 (1996) 1749–1758.
[24] W. Humphrey, A. Dalke, K. Schulten, VMD: Visual molecular dynamics, J. Mol. Graph. Model. 14 (1996) 33–38.
[25] F.A. Macleod, S.R. Guiot, J.W. Costerton, Electron microscopic examination of the extracellular polymeric substances in anaerobic granular biofilms, World J. Microb. Biot. 11 (1995) 481–485.
[26] L. Yang, Y. Hu, Y. Liu, J. Zhang, J. Ulstrup, S. Molin, Distinct roles of extracellular polymeric substances in Pseudomonas aeruginosa biofilm development, Environ. Microbiol. 13 (2011) 1705–1717.
[27] M. Domenech, E. Garcia, A. Prieto, M. Moscoso, Insight into the composition of the intercellular matrix of Streptococcus pneumoniae biofilms, Environ. Microbiol. 15 (2013) 502–516.
[28] P. Larsen, J.L. Nielsen, D. Otzen, P.H. Nielsen, Amyloid-like adhesins produced by floc-forming and filamentous bacteria in activated sludge, Appl. Environ. Microb. 74 (2008) 1517–1526.
[29] S. Szilveszter, B. Raduly, B. Abraham, S. Lanyi, In situ imaging of biopolymers and extracellular enzymes in activated sludge flocs of a municipal wastewater treatment plant, J. Chem. Technol. Biot. 88 (2013) 1295–1304.
[30] M.R. Chapman, L.S. Robinson, J.S. Pinkner, R. Roth, J. Heuser, M. Hammar, S. Normark, S.J. Hultgren, Role of Escherichia coli curli operons in directing amyloid fiber formation, Science 295 (2002) 851–855.
[31] H.C. Flemming, T.R. Neu, D.J. Wozniak, The EPS matrix: the "house of biofilm cells", J. Bacteriol. 189 (2007) 7945–7947.
[32] S. Jachlewski, W.D. Jachlewski, U. Linne, C. Brasen, J. Wingender, B. Siebers, Isolation of extracellular polymeric substances from biofilms of the thermoacidophilic archaeon sulfolobus acidocaldarius, Front. Bioeng. Biotechnol. 3 (2015) 123.
[33] Z.W. Wang, Y. Liu, J.H. Tay, Distribution of EPS and cell surface hydrophobicity in aerobic granules, Appl. Microbiol. Biotechnol. 69 (2005) 469–473.
[34] D. Sengupta, S. Datta, D. Biswas, Towards a better production of bacterial exopolysaccharides by controlling genetic as well as physico-chemical parameters, Appl. Microbiol. Biotechnol. 102 (2018) 1587–1598.
[35] B.V. Mohite, S.H. Koli, C.P. Narkhede, S.N. Patil, S.V. Patil, Prospective of microbial exopolysaccharide for heavy metal exclusion, Appl. Biochem. Biotechnol. 183 (2017) 582–600.
[36] S. Wang, L. Liu, H. Li, F. Fang, P. Yan, Y. Chen, J. Guo, T. Ma, Y. Shen, The branched chains and branching degree of exopolysaccharides affecting the stability of anammox granular sludge, Water Res 178 (2020), 115818.
[37] N.I. Abu-Lail, T.A. Camesano, Polysaccharide properties probed with atomic force microscopy, J. Microsc. 212 (2003) 217–238.
[38] J.S. Kavanaugh, C.E. Flack, J. Lister, E.B. Ricker, C.B. Ibberson, C. Jenul, D. E. Moormeier, E.A. Delmain, K.W. Bayles, A.R. Horswill, Identification of extracellular DNA-binding proteins in the biofilm matrix, mBio 10 (2019).
[39] H. Li, Y. Li, C. Li, Characterization of humic acids and fulvic acids derived from sewage sludge, Asian J. Chem. 25 (2013) 10087–10091.
[40] Y. Tang, X. Dai, B. Dong, Y. Guo, L. Dai, Humification in extracellular polymeric substances (EPS) dominates methane release and EPS reconstruction during the sludge stabilization of high-solid anaerobic digestion, Water Res 175 (2020), 115686.
[41] F. Fang, H.L. Hu, M.M. Qin, Z.X. Xue, J.S. Cao, Z.R. Hu, Effects of metabolic uncouplers on excess sludge reduction and microbial products of activated sludge, Bioresource Technol 185 (2015) 1–6.
[42] H. Wennerstrom, E. Vallina Estrada, J. Danielsson, M. Oliveberg, Colloidal stability of the living cell, Proc. Natl. Acad. Sci. U S A 117 (2020) 10113–10121.
[43] B. Frølund, T. Griebe, P.H. Nielsen, Enzymatic activity in the activated-sludge floc matrix, Appl. Microbiol. Biotechnol. 43 (1995) 755–761.
[44] D.R. de Graaff, S. Felz, T.R. Neu, M. Pronk, M.C.M. van Loosdrecht, Y. Lin, Sialic acids in the extracellular polymeric substances of seawater-adapted aerobic granular sludge, Water Res 155 (2019) 343–351.
[45] C.-C. Lee, D.-J. Lee, J.-Y. Lai, Labeling enzymes and extracellular polymeric substances in aerobic granules, J. Taiwan Inst. Chem. E. 40 (2009) 505–510.
[46] L. Wang, L. Wang, Q. Shi, H. Yu, Purification and molecular weight distribution of a key exopolysaccharide component of Bacillus megaterium TF10, J. Environ. Sci. 63 (2018) 9–15.
[47] L. Zhu, J. Zhou, M. Lv, H. Yu, H. Zhao, X. Xu, Specific component comparison of extracellular polymeric substances (EPS) in flocs and granular sludge using EEM and SDS-PAGE, Chemosphere 121 (2015) 26–32.
[48] F.X. Jia, Q. Yang, J.H. Han, X.H. Liu, X.Y. Li, Y.Z. Peng, Modeling optimization and evaluation of tightly bound extracellular polymeric substances extraction by sonication, Appl. Microbiol. Biotechnol. 100 (2016) 8485–8494.
[49] F. Fang, S.N. Wang, K.Y. Li, J.Y. Dong, R.Z. Xu, L.L. Zhang, W.M. Xie, J.S. Cao, Formation of microbial products by activated sludge in the presence of a metabolic uncoupler o-chlorophenol in long-term operated sequencing batch reactors, J. Hazard. Mater. 384 (2019), 121311.
[50] C. Feng, T. Lotti, Y. Lin, F. Malpei, Extracellular polymeric substances extraction and recovery from anammox granules: evaluation of methods and protocol development, Chem. Eng. J. 374 (2019) 112–122.
[51] C. Pellicer-Nacher, C. Domingo-Felez, A.G. Mutlu, B.F. Smets, Critical assessment of extracellular polymeric substances extraction methods from mixed culture biomass, Water Res 47 (2013) 5564–5574.
[52] L. Wei, J. Li, M. Xue, S. Wang, Q. Li, K. Qin, J. Jiang, J. Ding, Q. Zhao, Adsorption behaviors of Cu(2+), Zn(2+) and Cd(2+) onto proteins, humic acid, and polysaccharides extracted from sludge EPS: sorption properties and mechanisms, Bioresource Technol. 291 (2019), 121868.
[53] L. Huang, M. Li, G. Si, J. Wei, H.H. Ngo, W. Guo, W. Xu, B. Du, Q. Wei, D. Wei, Assessment of microbial products in the biosorption process of Cu(II) onto aerobic granular sludge: Extracellular polymeric substances contribution and soluble microbial products release, J. Colloid Interface Sci. 527 (2018) 87–94.
[54] X. Li, X. Zeng, D. Qiu, Z. Zhang, X. Zhang, Z. Shao, Extracellular electron transfer in fermentative bacterium Anoxybacter fermentans DY22613(T) isolated from deep-sea hydrothermal sulfides, Sci. Total Environ. 722 (2020), 137723.
[55] C. Echeverria, M.T. Torres, M. Fernandez-Garcia, C. de la Fuente-Nunez, A. Munoz-Bonilla, Physical methods for controlling bacterial colonization on polymer surfaces. Biotechnol. Adv. (2020), 107586.
[56] M. Whiteley, S.P. Diggle, E.P. Greenberg, Progress in and promise of bacterial quorum sensing research, Nature 551 (2017) 313–320.
[57] M. Marouf, P. Machart, V. Bansal, C. Kilian, D.S. Magruder, C.F. Krebs, S. Bonn, Realistic in silico generation and augmentation of single-cell RNA-seq data using generative adversarial networks, Nat. Commun. 11 (2020) 166.
[58] S. Felz, S. Al-Zuhairy, O.A. Aarstad, M.C. van Loosdrecht, Y.M. Lin, Extraction of structural extracellular polymeric substances from aerobic granular sludge, J. Vis. Exp. (2016).